Synergistic Effect of Compatibilizer and Cloisite 30B on the Functional Properties of Poly(3-hydroxybutyrate-co-3-hydroxyvalerate)/Polylactide Blends

Idris Zembouai, Stephane Bruzaud, Mustapha Kaci, Aida Benhannida, Yves-Marie Corre, Yves Grohens, José-Marie Lopez-Cuesta

Synergistic Effect of Compatibilizer and Cloisite 30B on the Functional Properties of Poly(3-hydroxybutyrate-*co*-3-hydroxyvalerate)/Polylactide Blends

Idris Zembouai,[1,2] Stéphane Bruzaud,[2] Mustapha Kaci,[1] Aida Benhamida,[1] Yves-Marie Corre,[2] Yves Grohens,[2] José-Marie Lopez-Cuesta[3]

[1] *Laboratoire des Matériaux Polymères Avancés (LMPA), Université Abderrahmane Mira, Faculté de Technologie, Bejaia 06000, Algeria*

[2] *Laboratoire d'Ingénierie des Matériaux de Bretagne (LIMATB), Université de Bretagne-Sud, Rue de Saint Maudé, 56321 Lorient Cedex, France*

[3] *Centre de Recherche C2MA, Ecole des Mines d'Alès, 6 avenue de Clavières, 30319 Alès Cedex, France*

Blends of poly(3-hydroxybutyrate-*co*-3-hydroxyvalerate) (PHBV) and polylactide (PLA) with different PHBV/PLA weight ratios (100/0, 75/25, 50/50, 25/75, 0/100) were prepared by melt compounding. To improve the miscibility between the two components of the blend, low amount of compatibilizing agent (5 wt%), obtained by grafting maleic anhydride onto PHBV, was used. When compared with the uncompatibilized blends, the compatibilizer presence induces a greater interfacial adhesion. The effect of Cloisite 30B (C30B) on the blend morphology and the blend properties was also investigated. The morphology of the different blends as well as the evolution of their material properties were discussed in terms of the nanoclay and compatibilizing agent contents. A synergistic effect of compatibilizer and C30B was highlighted leading to an improved miscibility of the two blend components. The resulting properties were correlated with the morphology observed for the different blends.

INTRODUCTION

During this last decade, much attention has been focused on both biodegradable polymers that can be produced from renewable resources and polymer layered silicate nanocomposites [1 3]. Among all these biobased and biodegradable polymers, polyhydroxyalkanoates (PHAs) and polylactide (PLA) are a part of the most promising polymers [4, 5]. PHAs represent an interesting alternative to synthetic polymers due to many advantages. Not only they are biodegradable and biocompatible, but they can also be produced by bacterial fermentation from renewable resources [4, 6]. Nevertheless, PHAs are not fully competitive compared with conventional thermoplastics since they exhibit high crystallinity, brittleness, and poor thermal stability just above their melting temperature [4]. PLA is one kind of thermoplastic aliphatic polyester derived from non-fossil renewable natural resources such as starch [5]. PLA has been used for many applications like the packaging industry and widely used in biomedical applications because of its biodegradability and biocompatibility but PLA has poor processing properties and are brittle at room temperature.

The interest in polymer blends is constantly increasing because this is an opportunity to finely adjust the final properties of the materials. Regarding publications on PHA/PLA blends reported in the literature, this process was explored as an alternative economical way of achieving novel materials with desired properties [7 10]. PHA/PLA polymer blends tend to phase separation due to immiscibility, resulting into poor properties. The compatibility between the polymer blend components has previously been enhanced by the addition of a third component of organic nature by the use of block and graft copolymers which improve the interfacial properties of two immiscible polymers and then stabilize the blend morphology [11].

Nanocomposites based on polymer blends have recently received special attention. One major part of the research has dealt with the effect of the nanoparticles on miscibility/compatibility and the microstructure of the polymer blends. The most important features that can affect the role and performance of the nanoparticles in

Correspondence to: Stéphane Bruzaud; e mail: stephane.bruzaud@univ ubs.fr
Contract grant sponsor: EGIDE (TASSILI Program); contract grant num ber: 12 MDU 871.

the polymer blends are their localization, their interactions with polymer components and the dispersion state in the polymer matrix [12 14].

As example of compatibization, Kumar et al. [15] prepared blends based on PLA and poly(butylene adipate terephtalate) (PBAT) using glycidyl methacrylate (GMA) as a reactive compatibilizer to improve the interfacial adhesion between PLA and PBAT. Their results revealed that a PLA/PBAT blend with 25 wt% PBAT exhibited the highest impact strength. Moreover, incorporation of GMA and nanoclay in the blend caused a great increase in the impact strength compared with PLA/PBAT blend. Hong et al. [16] also reported that the nanoclay incorporation into an immiscible polymer blends stabilizes the phase morphology due to the compatibilization effect. They investigated the interfacial tension reduction in poly(butylene terephtalate)/polyethylene/clay blend [17]. The results showed that the nanoclay located at the interface significantly influences the blend morphology such as droplet size or droplet size distribution. These morphological changes are caused by the compatibilization effect of nanoclay involved in the interfacial tension reduction. Ray et al. [18] studied the role of organically layered silicates as compatibilizers for the immiscible polystyrene/polypropylene blends. They concluded that the organoclay not only acts as filler but also as a compatibilizer.

In a recent article, poly(3-hydroxybutyrate-*co*-3-hydroxyvalerate) (PHBV) and PLA blends were prepared by melt mixing without any compatibilizer or filler [10]. It was concluded that PHBV/PLA blends form a biphasic system over the whole composition range. Despite this immiscibility between the two polymers, it has shown that the production of blends based on PHBV and PLA can be an efficient and promising route to extend their applications as biodegradable materials, considering the possibility to finely tune their functional properties by adjusting the respective proportions of each component [10]. To improve and/or modulate the properties of biodegradable polymers like PLA or PHAs, the elaboration of hybrid systems based on nanoclays associated to the polymer blend strategy seems to be a promising solution [1, 3, 6, 19, 20]. In this article which is a continuation of the previous work [10, 21], we report the coupled effects of nanoclay and compatibilizer on the blend morphology. The consequences in terms of thermal stability, flammability, mechanical properties and rheological behavior will be investigated.

EXPERIMENTAL SECTION

Materials Used

PLA was supplied in pellets form by NatureWorks under the trade name 7001D. The polymer is a semicrystalline one having the following main properties: density = 1.25 g cm $^{-1}$, MFI = 6 g/10 min (210°C, 2.16 kg), T_g = 60°C and T_m = 160°C.

PHBV was manufactured by Tianan Biological Materials Co. Ltd. (China) and commercialized in pellets form under the trade name ENMAT Y1000P. According to the manufacturer, PHBV has the following properties: density = 1.25 g cm $^{-1}$, T_g = 8°C and T_m = 165°C. This grade has been comprehensively characterized in a recent article [4].

Cloisite 30B (C30B) is an organically modified montmorillonite which is commercially available and was supplied by Southern Clay Products (Texas). C30B is a montmorillonite modified with *bis*-(2-hydroxyethyl) methyl tallow alkyl ammonium cations. C30B was dried under vacuum at 60°C for at least 24 h before use.

Maleic anhydride (MA) and dicumyl peroxide were purchased from Sigma-Aldrich and used as received.

Grafting of MA Onto PHBV

The grafting of MA onto PHBV was carried out according to the process described by Salim et al. [22]. Maleated PHBV was prepared by mixing 48.5 g of PHBV with 1.5 g of MA and 0.75 g of dicumyl peroxide, at 180°C, in a Brabender Plasticorder mixer (model W 50 EHT) which have the following characteristics: chamber volume of 55 cm^3, sample weight of 40 to 70 g, maximum torque of 200 N and maximum temperature equal to 500°C.mixer. The rotor speed was set at 30 rpm for 3 min in the early stage of the blending, and was increased progressively to 40 rpm for 5 min when MA and dicumyl peroxide were added. Finally, the blended samples were collected and dried under vacuum at 100°C to remove the non-reacted MA.

Preparation of PHBV/PLA Blends and PHBV/PLA/C30B Nanocomposites

Before use, all materials were dried under vacuum at 60°C for 24 h. Drying is necessary to minimize the hydrolytic degradation of the polymers during the melt processing in the extruder. The different samples were prepared by melt mixing in the mixer previously described. Different formulations based on PHBV/PLA blend with 3 and 5 wt% of C30B contents were prepared. The compatibilized PHBV/PLA/C30B nanocomposites were prepared by adding 5 wt% of PHBVMA. The major processing parameters were mixing temperature, screw speed and residence time; they were set at 180°C, 50 rpm and 8 min, respectively.

Technical Characterization

Fourier Transform-Infrared Spectroscopy (FT-IR). FT-IR spectra of various film samples based on PHBV and PHBVMA were recorded using a FT-IR spectrometer (Shimadzu 8400 M) using 4 cm $^{-1}$ resolution and 40 scans. All spectra were recorded in the transmittance mode in the 4000 to 400 cm $^{-1}$ region.

Differential Scanning Calorimetry (DSC). DSC analyzes were performed on weighted samples of about 10 mg, using a calorimeter (Mettler-Toledo DSC-882). The samples were first heated from 40 to 200°C at a heating rate of 10°C min ^{1} under nitrogen atmosphere and maintained at this temperature for 2 min to eliminate thermal history. The samples were then cooled to 40°C at a cooling rate of 10°C min ^{1}. Then the samples were reheated to 200°C at 10°C min ^{1} so that the melting could be studied.

Scanning Electron Microscopy (SEM). Morphologies were observed with a scanning electron microscope (Jeol JSM-6031) to examine the fracture surface of the samples. The neck region for the broken specimens fractured in liquid nitrogen is parallel to the draw direction in order to reveal the internal morphology. Before observation, the fracture surfaces were coated with a thin gold layer by means of a polaron sputtering apparatus (Polaron E5100).

Wide-Angle X-ray Scattering (WAXS). The WAXS measurements were performed at room temperature using advance diffractometer equipment (Bruker AXS D8), operating at the CuKα radiation (wavelength $\lambda = 0.154$ nm) for 40 kV and 40 mA. The 2θ scan range was used from 2° to 10° at a scan speed of 40 step s ^{1}.

Rheological Measurements. Oscillatory shear measurements were performed using a controlled stress rheometer (Anton Paar Rheometer MCR 301) equipped with parallel disks of 25 mm diameter using a gap of 1.5 mm. Sample disks were vacuum dried at 60°C for 24 h before testing. Strain sweep viscoelastic tests were first performed at a fixed angular frequency of 1 Hz in order to determine the extent of the linear regime; then, frequency sweep experiments were carried out at a fixed strain in the linear regime in order to determine the linear viscoelastic moduli, G' and G'', as well as the complex viscosity η^*. The angular frequencies were swept from 100 to 0.01 Hz with five points per decade at temperatures of 175°C. All rheometrical data obtained were shown to be reproducible within $\pm 5\%$.

Thermogravimetric Analysis (TGA). TGA experiments were carried out in a thermal analyzer (Setaram TGDTA 92-10) using a scanning rate of 10°C.min ^{1} under nitrogen in the temperature range starting from 20°C up to 600°C.

Pyrolysis Combustion Flow Calorimeter (PCFC). PCFC apparatus (FTT) was used to pyrolyze (3 ± 1) mg of sample by heating up to 780°C at a heating rate of 1°C s ^{1} under a nitrogen flow, and the gases produced during pyrolysis were sent into a combustor and burnt at a temperature of 900°C in the presence of oxygen (20%). The heat release rate (HRR) of samples and the peak of HRR (PHRR) were noted and each measurement was performed at least five times (up to 10 times). The results were averaged with an error of less than 5%, while the error on temperature of the P_{HRR} (T_{PHRR}) measurement is less than 1%. The gases produced at the temperature of PHRR observed during the PCFC test were characterized.

Tensile Testing. The static tensile tests were carried out in a laboratory where the temperature was 23°C and the humidity was 48% according to ISO 527 using a testing apparatus (MTS Synergie RT1000). The loading speed was 1 mm min ^{1}. An extensometer was used with a nominal gauge length of 25 mm. The dumbbell-shaped samples with a dimension of $75 \times 4 \times 1$ $(mm)^3$ were stamped from the compression molded sheets, using a hydraulic press equipped with two heated plates at 180°C with a pressure of 30 bars for 3 min. The tests were carried out at least five times for each material and the results were averaged arithmetically.

Dynamic Mechanical Analysis (DMA). The thermomechanical behavior of polymer samples has been investigated using a dynamical mechanical analyzer (TA Instruments DMA 2980). The specimen was a thin rectangular strip with dimensions around $30 \times 6 \times 2$ $(mm)^3$ prepared from the compression molded sheets, using a hydraulic press equipped with two heated plates at 180°C with a pressure of 30 bars for 3 min. A temperature scan from 40°C up to 150°C was performed at the rate of 3°C min ^{1} while a dynamic tensile test was performed at a frequency of 10 Hz with an amplitude of 10 μm.

RESULTS AND DISCUSSION

Grafting of MA on the PHBV and Characterization of Maleated PHBV

In order to increase the compatibilization between PHBV and C30B, a proper coupling agent was prepared. In particular, PHBV was modified by MA grafting (5 wt%) onto polymeric backbone through the thermal decomposition of dicumylperoxide, according to Scheme 1.

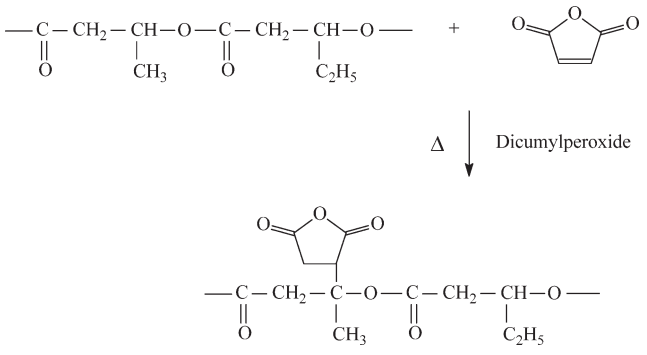

SCHEME 1.

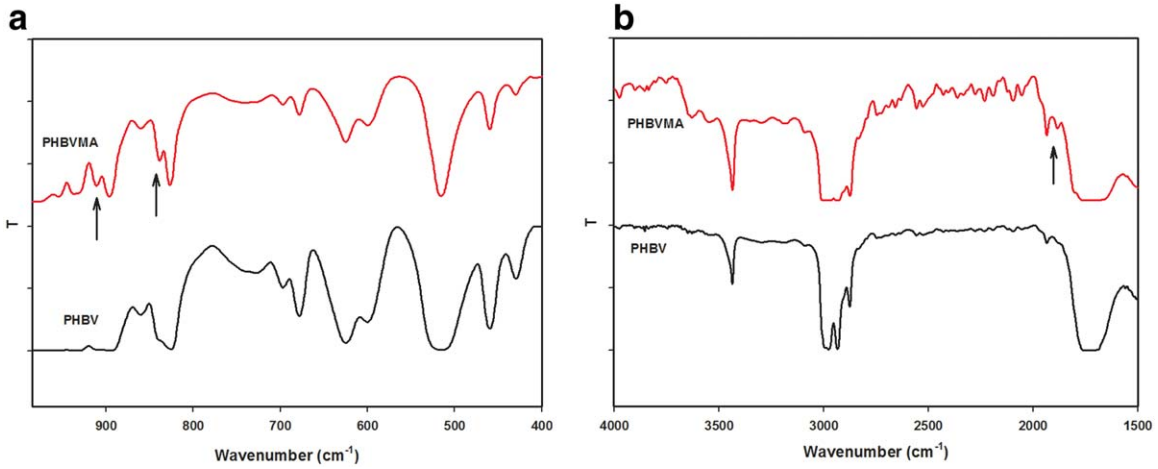

FIG. 1. FT IR spectra of neat PHBV and PHBVMA (a): 1000 400 cm ^{1} and (b): 4000 to 1500 cm ^{1}. [Color figure can be viewed in the online issue, which is available at wileyonlinelibrary.com.]

The insertion of MA mainly occurs onto hydroxybutyrate units, probably due to statistical, steric and chemical effects [23]. The grafting reaction was performed in bulk in order to avoid the use of organic solvent.

The grafting reaction of MA was monitored by FT-IR analysis. In Fig. 1, different regions of FT-IR spectra of neat PHBV and grafted PHBV at 5 wt% are reported. As it can be observed, new absorption bands centered at 1855, 911, and 820 cm ^{1} appear in the spectra of grafted PHBV. These bands can be attributed to the asymmetric stretching of the MA carbonyl group and to the bending of the CH group of grafted anhydride ring, respectively, thus confirming the occurred reaction [23].

To evaluate the effects of the process and the grafting reaction on the possible PHBV degradation, rheological measurements were performed on neat PHBV and PHBV grafted with 5 wt% of MA. The viscoelastic properties are reported in Fig. 2.

The decrease in complex viscosity and in storage modulus versus frequency is believed to be the result of a decrease in molecular weight. The grafting reactions lead to a partial PHBV degradation as previously observed by Avella et al. [23].

The effect of MA on the thermal properties of maleated PHBV (PHBVMA) was investigated by DSC (Fig. 3).

The results from DSC analysis show that PHBV has endothermic melting temperature (T_m) at 174°C. In the case of PHBVMA, two endothermic melting temperatures (T_{m1} and T_{m2}) at 160 and 167°C appear in the curve and could be a result of the recrystallization phenomenon during melting associated to partial PHBV degradation. The melting temperature of PHBVMA decreased comparatively to the T_m of neat PHBV. A slight reduction was also observed in the crystallization temperature (T_c) of maleated PHBV. At the same time, the glass transition temperature (T_g) of PHBVMA shifts to lower temperature ($T_g =$ 3.4°C for PHBVMA) comparatively to $T_g = 2.8$°C obtained for PHBV. There is a possibility of steric hindrance and disruption of MA groups to the molecular

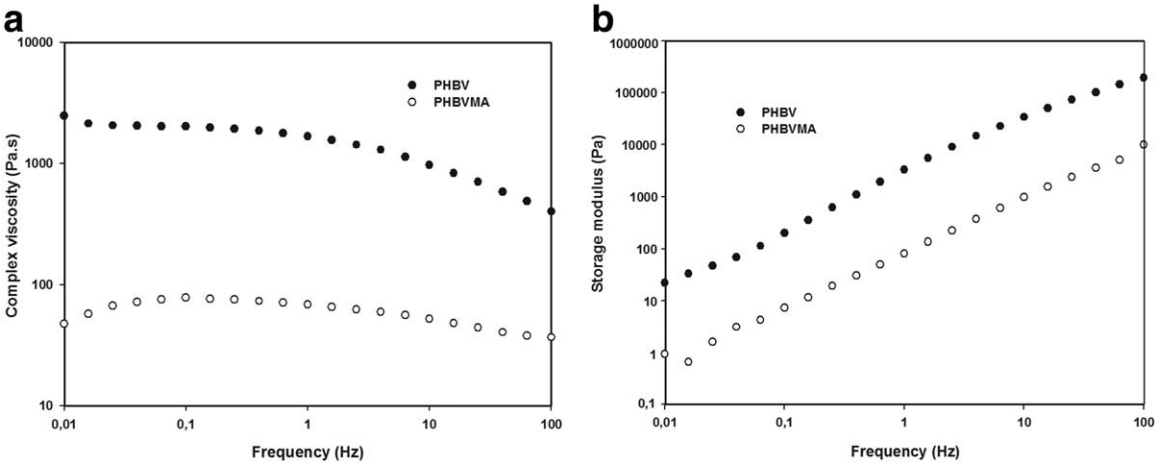

FIG. 2. (a) Complex viscosity and (b) storage modulus of PHBV and PHBMA at 175°C under 2% of dynamical shear strain.

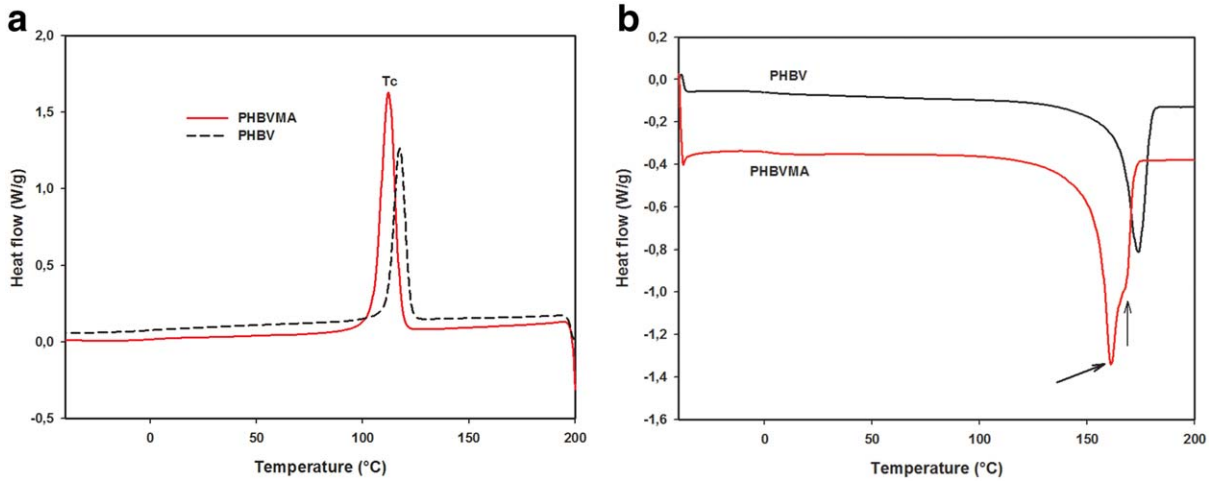

FIG. 3. DSC thermograms of neat PHBV and PHBVMA (a): cooling cycle at 10°C min ^{1} and (b): 2nd run. [Color figure can be viewed in the online issue, which is available at wileyonlinelibrary.com.]

linearity of PHBV. The chains were able to rotate the molecule at a lower energy, which led to branching and larger total free volume [24].

Nanocomposite Characterization

Morphology of PHBV-PLA-C30B Nanocomposites. PHBV/PLA blends exhibit separated phase morphology and there is a poor adhesion at the interfaces, as described in the last article [10]. The separated phase morphology is discernible, signifying immiscibility between the two biopolymers. Figure 4a,b,c show some SEM micrographs of the fractured surface of PHBV/PLA 25/75, PHBV/PLA 25/75 at clay loading of 3 wt%, without and with PHBVMA compatibilizer, respectively.

The comparison of the different micrographs suggests a drastic change in the material morphology. By the addition of 3 wt% of C30B (without PHBVMA compatibilizer), the dispersed phase becomes more deformed and less discernible and the morphology was rather co-

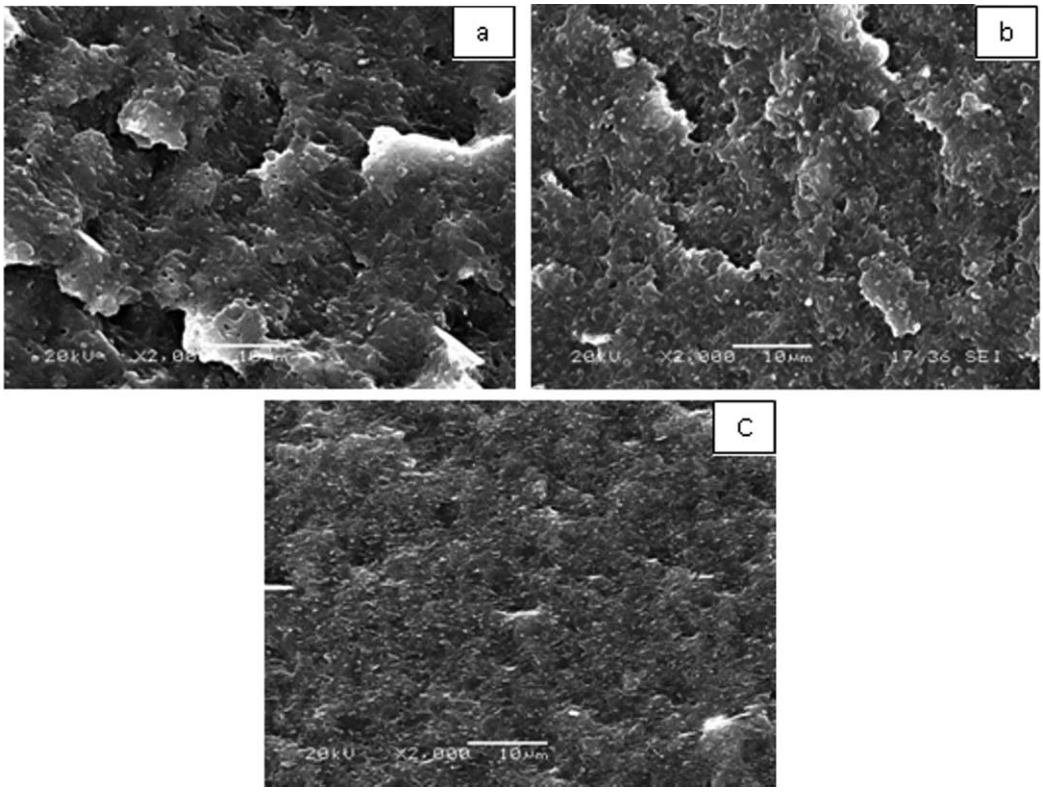

FIG. 4. SEM micrographs of fractured surface of PHBV/PLA 25/75 (a), PHBV/PLA 25/75 with 3 wt% of C30B (b), PHBV/PLA 25/75 with 3 wt% of C30B and 5 wt% of PHBMA compatibilizer (c).

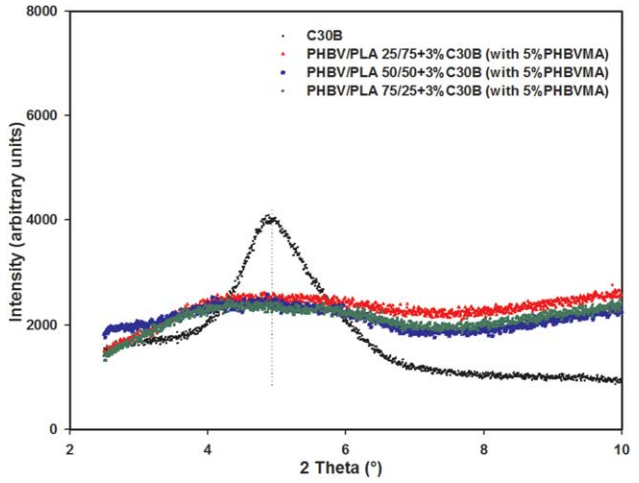

FIG. 5. WAXS patterns of C30B and PHBV/PLA blends with 3 wt% of C30B and 5 wt% of PHBVMA compatibilizer. [Color figure can be viewed in the online issue, which is available at wileyonlinelibrary.com.]

continuous. It is not easy to distinguish the phases and the nearly phase-separated domains are not visible. The morphology can be considered as relatively homogeneous at this magnification, suggesting a change in the miscibility between the two blend components in the presence of C30B. The SEM image of the fractured surface of PHBV/PLA 25/75 at a clay loading of 3 wt% with PHBVMA compatibilizer reveals that the compatibilizer incorporation into the PHBV/PLA blend nanocomposites changes the co-continuous to a dispersed-type morphology. This can be attributed to the reduction of interfacial tension of the system due to increased interfacial interactions between the blend components and to the localization of the clay in the blend due to the chemical linkage. The droplet sizes are noticeably reduced and this reduction in droplet size may be attributed to the formation of an interphase resulting from the migration of PHBVMA to the interfacial area. This induces a relatively homogeneous morphology. These results indicate the efficiency of C30B and PHBVMA in improving the interfacial adhesion and the miscibility between PHBV and PLA.

Due to its ease and availability, WAXS is the most commonly used to probe nanocomposite structure, and the position, shape, and intensity of the different peaks may be allowed to evaluate the dispersion of mineral sheets within the polymer matrix (intercalated and/or exfoliated structures) [19]. WAXS patterns of C30B powder and PHBV/PLA blend nanocomposites with PHBVMA compatibilizer were presented in Fig. 5.

The WAXS pattern of C30B shows a diffraction peak at 4.8°, corresponding to a basal spacing. The *d*-spacing values (basal distance between clay layers) were calculated using Bragg's law ($\lambda = 2d\sin\theta$; d is the interlayer d-spacing and λ is the wave length). The d_{001} peak of C30B appears at $2\theta = 4.8°$, corresponding to an interlayer spacing of 1.8 nm. No peak is observed in the WAXS patterns between 2 and 10° for the obtained PHBV/PLA blend nanocomposites with PHBVMA compatibilizer, probably suggesting the formation of nanocomposite structures more or less exfoliated. However, the disappearance of a diffraction peak cannot always be directly attributed to an exfoliated morphology. For these reasons, WAXS analysis is not sufficient for a complete morphological characterization of the nanocomposites and rheological studies are required for a better understanding of the internal structure and the C30B dispersion in the matrix (see below).

Thermal Properties. The properties of the nanocomposites PHBV/PLA/C30B can be significantly affected by the crystallization characteristics of PHBV and PLA. Table 1 summarizes the thermal data obtained for all the samples through DSC experiments during a cooling scan and a second heating cycle. The main thermal parameters are as follows: the crystallization temperature (T_c), the crystallization enthalpy (ΔH_c), the glass transition temperature (T_g), the cold crystallization temperature (T_{cc}) and the cold crystallization enthalpy (ΔH_{cc}). The melting

TABLE 1. Thermal characteristics of neat PHBV, neat PLA, PHBV/PLA blends, and PHBV/PLA/C30B determined by DSC.

Samples	Clay (wt%)	PHBVMA (wt%)	$T_{c,PHBV}$ (°C)	$\Delta H_{c,PHBV}$ (J g^{-1})	$T_{cc,PLA}$ (°C)	$\Delta H_{cc,PLA}$ (J g^{-1})	$T_{g,PHBV}$ (°C)	$T_{g,PLA}$ (°C)	$T_{m,PHBV}$ (°C)	$T_{m,PLA}$ (°C)	$\Delta H_{m,PHBV}$ (J g^{-1})	$\Delta H_{m,PLA}$ (J g^{-1})
PHBV			118.3	46.5			2.8		174.0		51.6	
	3		119.8	73.0			1.1		172.0		84.7	
PHBV/PLA 75/25			116.7	49.5	119.9	3.2	3.0	57.1	173.1	151.2	45.6	16.3
	3		118.3	54.1	112.5	4.5		54.8	170.3	151.0	51.2	19.1
	3	5	117.5	81.0	109.8	6.0		55.8	172.0	150.1	64.5	25.2
PHBV/PLA 50/50			115.6	40.7	125.1	7.8	3.3	57.9	172.8	152.6	39.3	17.8
	3		115.0	35.5	116.3	10.7		55.2	171.3	150.2	46.7	21.4
	3	5	116.1		113.2				171.4	151.4	57.8	25.5
PHBV/PLA 25/75			117.9	00.6	124.3	12.6	4.5	58.4	170.1	152.5	4.1	10.0
	3		116.1	01.9	121.0	23.3		56.7	169.4	151.8	6.7	18.2
	3	5	108.1	11.5	115.8	25.5		57.0	170.0	152.7	13.2	25.8
PLA					118.0	17.2		59.8		154.3		17.8
	3				117.3	27.3		57.0		151.2		26.5

process is characterized by the melting temperature (T_m) and the melting enthalpy (ΔH_m).

Regarding the glass transition, two T_g are observed for the whole samples. This indicates phase immiscibility between PLA and PHBV. Moreover, it is noticeable that a T_g depression occurs for the nanocomposites compared with the nonreinforced ones. This may be due to the fact that the C30B has a significant influence on the chain flexibility and intermolecular attraction of PHBV/PLA blend [25]. However, the determination of the glass transition temperature of PHBV in the nanocomposites blends, compatibilized or not, was difficult according to the chosen heating rate. T_{cc} shifts to lower temperature for the uncompatibilized and compatibilized nanocomposites. This indicates that the clay particle acts as nucleating agent increasing the crystallization rate of PHBV/PLA blend. The clay particles seem to promote the mobility of PHBV/PLA chains and the rearrangements of the macromolecular chains during crystallization. The melting temperatures relative to PHBV and PLA slightly decrease for all the samples with the addition of C30B and PHBVMA compatibilizer indicating that the thermal behaviors of the blends are influenced by the presence of clay. Furthermore, ΔH_{cc} and ΔH_m values significantly increase with the addition of C30B and PHBVMA compatibilizer. It suggests that the clay favors the nucleation process considering that blend/clay interactions would induce a slight delay either into the melting or into the crystallization process.

Thermal Degradation Behavior. Thermal stability is a typical property for which the nanocomposite morphology plays an important role [26]. The thermal stability of polymeric materials is usually studied by TGA and the weight loss due to the formation of volatile products during degradation at a high temperature is monitored as a function of temperature. Generally, the incorporation of clay into the polymer matrix was found to enhance the thermal stability by acting as a superior insulator and mass transport barrier to the volatile products generated during decomposition [26]. The clay acts as a heat barrier, which enhances the overall thermal stability of the system, as well as an assistant for the formation of char after thermal decomposition.

TABLE 2. TGA results of neat PHBV, neat PLA, PHBV/PLA blends, and PHBV/PLA/C30B determined by DSC.

Samples	Clay (wt%)	$T_{degradation\ 5\%}$ (°C)	$T_{degradation\ 10\%}$ (°C)	$T_{degradation\ 50\%}$ (°C)	Char at 600°C (%)
PHBV		268	272	284	1.3
	3	274	277	291	3.3
PHBV/PLA 75/25		273	278	290	1.2
	3	282	287	301	3.1
PHBV/PLA 50/50		275	279	305	1.1
	3	286	293	317	2.8
PHBV/PLA 25/75		287	291	353	0.9
	3	295	301	354	2.8
PLA		332	341	362	0.3
	3	344	355	378	2.2

The significant data for the characterization of thermal stability are the onset temperature which is measured both by the temperature at which 5% and 10% degradation occurs, the mid-point of the degradation ($T_{degradation\ 50\%}$) and the fraction which is not volatile at 600°C, denoted as char. Thermogravimetric analyses were performed on the PHBV/PLA blends and PHBV/PLA/C30B nanocomposites to determine the influence of the addition of clay on the thermal stability. The comparison of TGA results between PHBV/PLA blends and PHBV/PLA/C30B nanocomposites indicates significant differences in thermal stability (Table 2 and Fig. 6).

The thermal stability of nanocomposites containing only 3 wt% of C30B is higher than the corresponding unfilled blend. From Table 2, the thermal stability of neat PHBV, neat PLA and PHBV/PLA blends

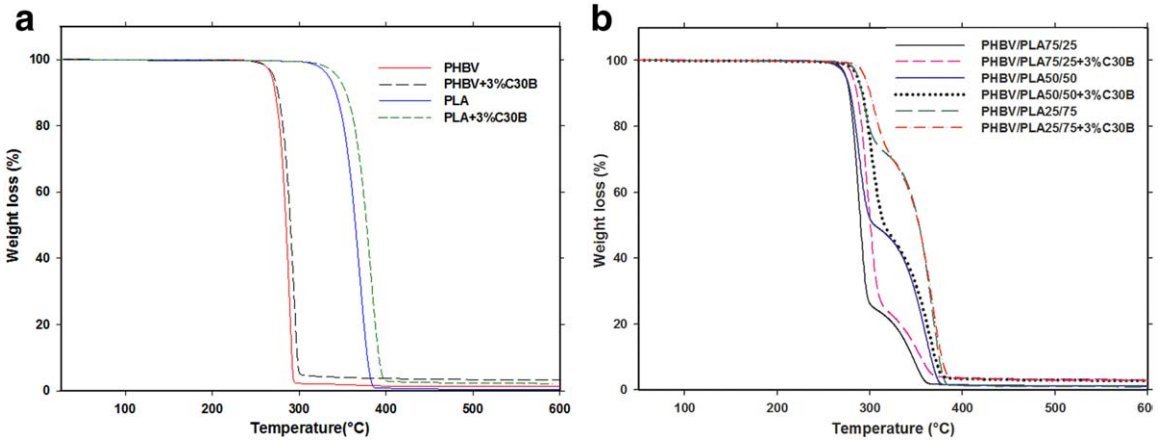

FIG. 6. Influence of C30B on TGA curves for (a) PHBV and PLA and (b) PHBV/PLA blends. [Color figure can be viewed in the online issue, which is available at wileyonlinelibrary.com.]

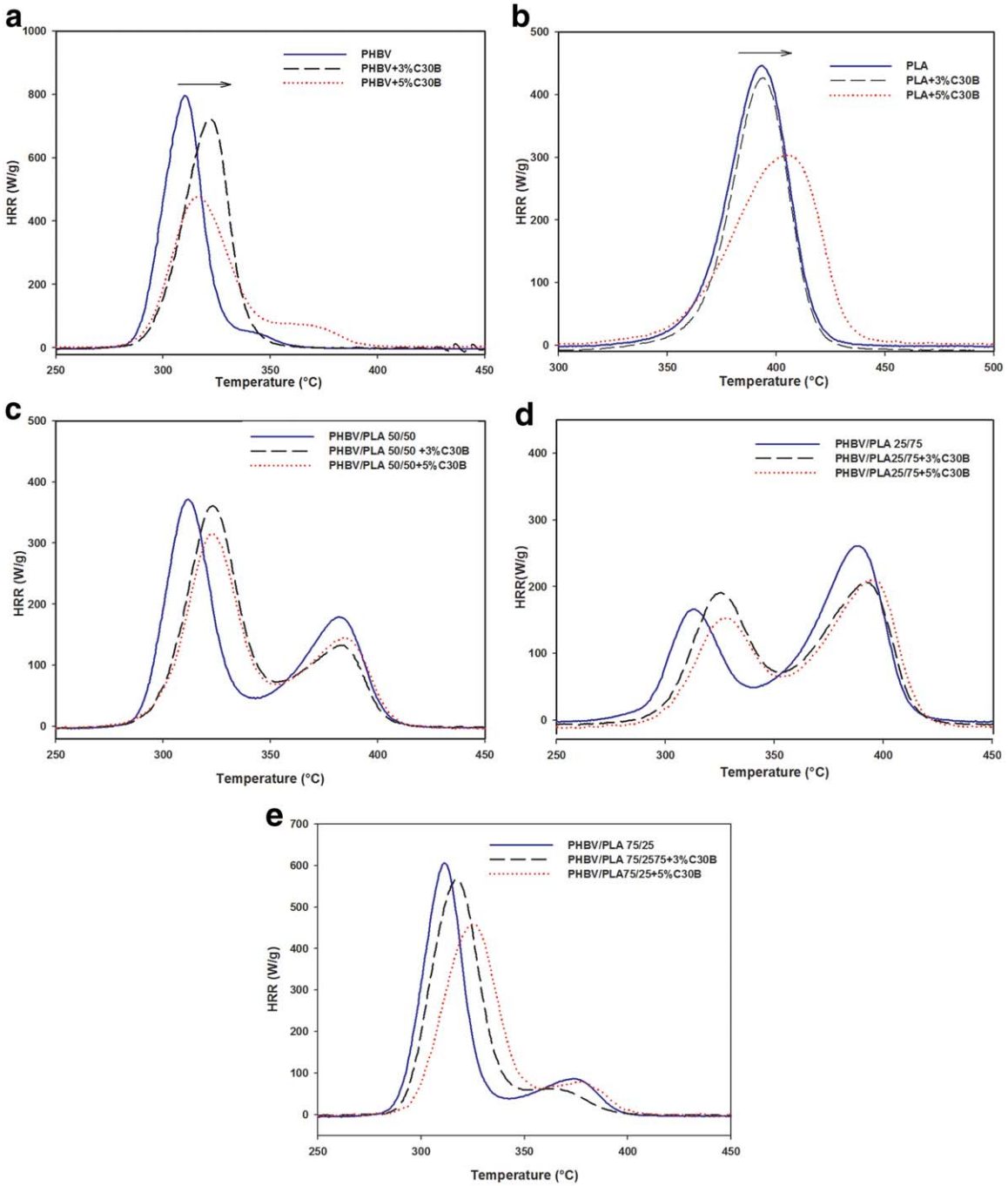

FIG. 7. Influence of C30B on HRR curves for (a) PHBV, (b) PLA, (c) PHBV/PLA 50/50, (d) PHBV/PLA 25/75, and (e) PHBV/PLA 75/25. [Color figure can be viewed in the online issue, which is available at wileyonlinelibrary.com.]

systematically increases with the addition of 3 wt% of C30B. For all nanocomposite samples, an increase by 6 to 12° C of the temperature at 5% weight loss and by 5 to 14°C of the temperature at 10% weight loss can be noticed when comparing with the corresponding blends. Furthermore, a significant increase of the temperature at 50% weight loss is observed in the presence of C30B. This increase can be associated to the presence of the nanodispersed clay phase. The decomposition shift to higher temperatures can be explained by a decrease in the diffusion of oxygen and volatile degradation products throughout composite material due the homogeneous incorporation of clay sheets [26, 27]. In addition, the decomposition temperature range is enlarged with C30B, which suggests that degradation is slowed down, probably due to the presence of

TABLE 3. HRC, THR and EHC from PCFC tests of neat PHBV, neat PLA, PHBV/PLA blends, and PHBV/PLA/C30B.

Samples	Clay (wt%)	HRC (J g $^{-1}$ K $^{-1}$)	THR (kJ g $^{-1}$)	Residu (%)	EHC (kJ g $^{-1}$)
PHBV		798	19.2	1.3	19.45
	3	757	18.5	3.4	19.15
	5	530	17.9	3.9	18.62
PHBV/PLA 75/25		715	17.9	1.0	18.08
	3	646	18.4	3.0	18.96
	5	565	17.7	4.1	18.45
PHBV/PLA 50/50		573	16.7	0.8	16.93
	3	543	16.0	3.3	16.54
	5	521	15.9	3.7	16.51
PHBV/PLA 25/75		471	15.4	0.6	15.49
	3	450	15.4	3.2	15.90
	5	427	15.1	3.9	15.71
PLA		444	15.5	0.3	15.54
	3	428	14.6	2.2	14.92
	5	295	14.4	3.6	14.93

very small and well-dispersed C30B sheets in the PHBV/PLA blend samples. The well-dispersed nanofillers then appear as effective barriers to heat and volatile compound diffusion and thus can counterbalance the degradation effect.

Flammability Properties. The pyrolysis combustion flow calorimeter (PCFC) is a relevant tool for assessing the flammability of fire retardant polymers at a microscopic scale [28]. The PCFC test was performed in order to evaluate the fire retardant mechanism of PHBV/PLA/C30B nanocomposites compared with the blend without C30B. The PCFC curves are presented in Fig. 7 and the characteristic data obtained from PCFC test of PHBV/PLA blend and its nanocomposites reinforced with 3 and 5 wt% of C30B are summarized in Table 3.

The heat release rate (HRR), total heat released (THR), effective heat of combustion (EHC), and the heat release capacity (HRC), in particular was found to be the most important parameters to evaluate fire safety [29, 30]. HRC is the ratio of the peak of HRR (or the sum of the peaks) to the selected temperature ramp (°C s $^{-1}$). This value is maximum for pristine PHBV and minimum for pristine PLA. HRC regularly decreases in function of the PLA fraction as well as THR and EHC. The temperature corresponding to the peaks for each polymer (PHBV at 308°C, PLA at 393°C) remains unchanged for the PHBV in the unfilled blends, but slightly decreases for PLA (the shift increases when the percentage of PLA decreases; 21°C is the maximum value, observed for the PHBV/PLA 75/25 composition), showing that the blend microstructure or processing steps could have an influence on PLA degradation.

The presence of C30B leads to a strong reduction in HRC and this reduction is the highest for 5 wt% of clay. The decrease of HRC for the filled compositions is lower for the polymer blends than for PHBV and particularly for PLA. Moreover, it can be noticed that the peak of HRR (pHRR) corresponding to PHBV is always shifted toward higher temperatures in presence of C30B, while it is not generally the case for the pHRR corresponding to PLA. Consequently, it can be suggested that C30B improves the fire reaction of PHBV in the blend by modifying its degradation pathway as well as promoting the formation of a physical barrier for volatile combustible by creating a tortuous path for migration owing to the aspect ratio of the particles [31, 32]. A ceramic layer is formed at the surface of the material in which the efficiency is dependent on the homogeneity of the forming layer [33]. The same mechanisms could be proposed for the thermal degradation of PLA, but mainly for PLA alone, since the pHRR temperature shifts seems less important or not significant in blends to be ascribed to a modification of the degradation pathway. Consequently, only the formation of a physical barrier seems to act on the fire reaction of PLA in the blend. These modifications of pHRR temperatures, only for PHBV in the filled blends, are in accordance with the TGA curves, which shows that C30B confers a better thermal stability to PHBV (shift of around 15°C), conversely to PLA. Hence, it can also be suggested that the blend morphology and the location of the silicate sheets in the blend could influence the mechanism of degradation of each blend component.

Finally, it has to be noticed that the amount of residues corresponds roughly to the inorganic content of C30B. Consequently, only a small quantity of char is formed.

Dynamic Mechanical Properties. DMA is a thermomechanical analysis used to study the viscoelastic properties of the polymers. It mainly gives information about the storage and loss moduli. The storage modulus is the inherent property which determines the dynamic rigidity originating from the elastic response of the material. The loss modulus is the viscous response of the material. Figure 8a,b shows the temperature dependence from 40°C to 130°C of these last parameters of PHBV/PLA blends and PHBV/PLA/C30B nanocomposites with and without compatibilizer.

The storage modulus of the PHBV/PLA/C30B nanocomposites improves in almost all the temperature range, in comparison with the unfilled ones (Fig. 8a). This observation may be due to the significant degree of intercalation of polymer chains into the silicate layers. The increase in the storage modulus is higher for previously compatibilized nanocomposites compared with uncompatibilized nanocomposites, suggesting that the compatibilization of the blends with C30B is more effective in the presence of 5 wt% of PHBVMA as compatibilizer. These results reveal that a good dispersion of C30B gives rise to a better performance of PHBV/PLA blends.

In the presence of PHBVMA compatibilizer, the PHBV/PLA/C30B nanocomposites exhibit higher storage modulus at temperatures below the glass transition of

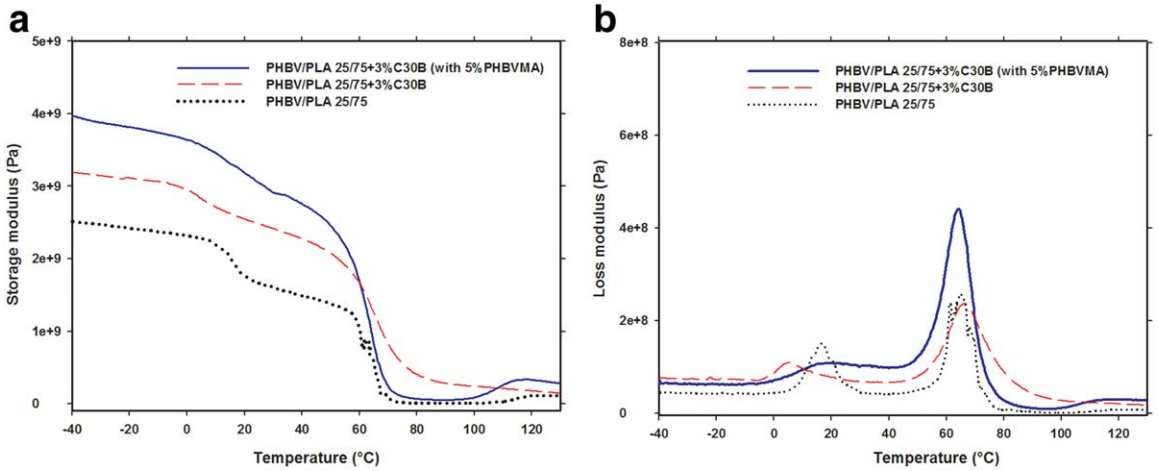

FIG. 8. Evolution of (a) dynamic storage modulus and (b) loss modulus. [Color figure can be viewed in the online issue, which is available at wileyonlinelibrary.com.]

PLA ($T_{g,PLA} = 59°C$), although these curves gradually decrease in storage modulus from around 15°C, which is associated to the glass transition of PHBV. It is observed that around PLA glass transition, the storage modulus of nanocomposites compatibilized with PHBVMA drastically decreases compared with the uncompatibilized ones. An explanation could be due to the presence of PHBVMA which shifts T_g to lower temperatures. T_g is usually interpreted as the peak of either the tan delta or the loss modulus curves obtained during the dynamic mechanical test [21]. From the loss modulus curves in Fig. 8b, the glass transition temperature appears at 62°C for compatibilized nanocomposites and at 67°C for the uncompatibilized nanocomposites. DMA is often employed to assess the miscibility of the polymer blends [34]. As shown in Fig. 8b, two distinct T_g are observed for blends. Nevertheless, in the special case of compatibilized nanocomposites with 5 wt% of PHBVMA, the T_g of PHBV is less distinguishable than in the case of PHBV/PLA blends or nanocomposites without compatibilizer. This seems to suggest that the compatibilizer presence noticeably contributes to improving the miscibility of PHBV/PLA blends.

Mechanical Properties. Even at a quite low ratio, nanoclays can act as excellent reinforcing agents for polymer materials if they are uniformly dispersed in the polymer matrix [1, 26]. Mechanical analysis of nanocomposites was performed to evaluate the influence of the clay with and without PHBMA compatibilizer. The main mechanical results are reported in Table 4.

It is obvious that the incorporation of 3 wt% of C30B induces significant change in the mechanical properties of the PHBV/PLA blend. The incorporation of 3 wt% of C30B into PHBV/PLA blends leads to a significant increase of the Young's moduli of blends. The addition of 3 wt% of C30B leads to an improvement in the Young's modulus of PHBV/PLA blends equal to 16, 11, and 14 % for PHBV/PLA 75/25, PHBV/PLA 50/50, and PHBV/PLA 25/75, respectively. It is believed that the enhancement in the Young's moduli of blends may be due to the formation of supramolecular assemblies obtained by the presence of dispersed anisotropic nanoplatelets [26]. Furthermore, the Young's moduli of nanocomposite blends with 5 wt% of PHBVMA comptabilizer increase up to 27, 20 and 23% in PHBV/PLA 75/25, PHBV/PLA 50/50, and PHBV/PLA 25/75 wt%,

TABLE 4. Effect of C30B and compatibilizer on the tensile properties of PHBV/PLA blends.

Samples	Clay (wt%)	PHBVMA (wt%)	Stress at break (MPa)	Elongation at break (%)	Young modulus (MPa)
PHBV			33.9 ± 2.0	1.5 ± 0.1	2593.0 ± 93.0
PHBV/PLA 75/25			37.3 ± 2.6	1.6 ± 0.2	2453.6 ± 24.1
	3		31.5 ± 1.2	1.2 ± 0.7	2914.7 ± 110.7
	3	5	29.4 ± 1.8	1.0 ± 0.9	3363.2 ± 35.2
PHBV/PLA 50/50			44.6 ± 2.3	4.7 ± 0.7	2357.7 ± 210
	3		40.3 ± 2.6	2.8 ± 0.1	2649.7 ± 62.3
	3	5	33.2 ± 2.7	2.3 ± 0.1	2917.5 ± 27.5
PHBV/PLA 25/75			45.1 ± 1.5	7.0 ± 1.3	2212.1 ± 103
	3		41.1 ± 2.6	2.5 ± 0.1	2559.1 ± 42
	3	5	35.8 ± 7.1	2.8 ± 0.6	2887.3 ± 99.2
PLA			55.7 ± 1.7	5.5 ± 1.2	2175.0 ± 113.0

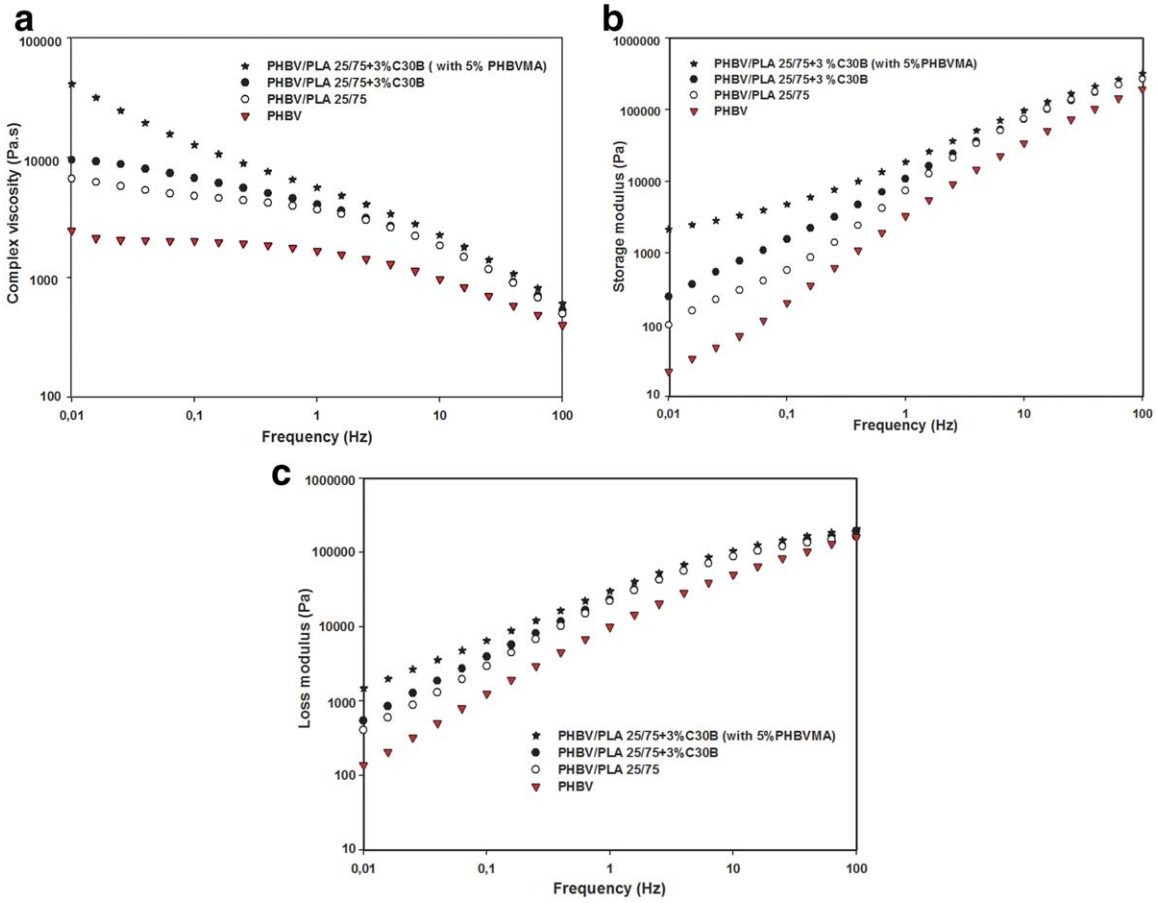

FIG. 9. Evolution of (a) complex viscosity, (b) storage modulus and (c) loss modulus at 175°C under 2% of dynamical shear strain. [Color figure can be viewed in the online issue, which is available at wileyonlinelibrary.com.]

respectively. The intensities of these polymer/clay interactions are higher in the case of compatibilized nanocomposites comparatively to uncompatibilized nanocomposites. The stronger interfacial interaction between the blend and the silicate layers induces a more pronounced improvement of the modulus value in the presence of 5 wt% of PHBVMA compatibilizer which favors the expansion of the gallery space of the reinforcing nanoclay by inclusion of polar groups intercalating between the clay layers through hydrogen bonding with the oxygen groups of clay [34 36].

The elongation at break of the nanocomposite blends is less as compared with their nonreinforced blends, independently of the compatibilizer presence. The filler presence may increase the stress concentration, which causes the composite to fail in a brittle manner resulting in the decrease of the elongation at break of the nanocomposite as compared with their pristine counterpart [34].

Concerning the evolution of the maximal stress at break which expresses the ultimate strength that the material can bear before break, the differences observed are sufficiently notable to draw some comments. The relationships between tensile stress, compatibility of blend components, filler/matrix interaction and dispersion are more complex than for the modulus, so no attempt is made at this time to justify the result with quantitative models [37]. Generally, the tensile stress of many nanocomposites has been found to increase with increased clay content [26]. However, in nanocomposites of PLA/C30B or poly(butylene succinate)/MMT, the opposite trends have also been reported [19, 38]. In the case of thermoplastic polyurethane-based nanocomposites containing C30B, upon silicate addition large improvements in stiffness were observed, which however were accompanied by a decrease in tensile stress [37]. The reason is not clear, but it is thought that the decrease in the tensile strength is attributed to the decrease in the elongation at break, which is probably related to the delamination of the polymer-silicate interlayer.

Rheological Properties. The embedding of nanosize clay particles into polymer matrices changes their rheological properties. The filler-polymer and the filler-filler interactions lead to an increase in the complex viscosity, particularly at low frequencies, and to a more pronounced shear-thinning behavior. Moreover, the matrix molecular weight and the degree of clay dispersion strongly affect the

rheological properties of the nanocomposites [39]. The region of linear viscoelastic behavior of polymers is greatly modified in the presence of the intercalated clay [40].

To study the C30B effect with and without PHBVMA on the rheological properties of PHBV/PLA blends, the complex viscosity, the storage modulus G' and the loss modulus G'' were investigated as a function of frequency. Figure 9 summarizes the results obtained for neat PHBV, PHBV/PLA 25/75 blend, PHBV/PLA 25/75 nanocomposite with 3 wt% of C30B and PHBV/PLA 25/75 nanocomposite with 3 wt% of C30B and previously compatibilized.

The incorporation of C30B in PHBV/PLA blend leads to a very impressive increase of the complex viscosity (Fig. 9a), the storage modulus (Fig. 9b) and the loss modulus (Fig. 9c). The comparison of the viscoelastic response of the materials shows the significant effect of the clay, particularly at low frequencies and this effect becomes even more substantial when 5 wt% of PHBVMA compatibilizer is used.

It is observed that the melts of PHBV/PLA/C30B nanocomposite exhibit higher G' compared than those of both neat PHBV and PHBV/PLA blend. This increase becomes more intense when the PHBVMA compatibilizer is added to the PHBV/PLA/C30B nanocomposite. At high frequencies, however, the G' of all the sample melts come close together, except for the neat PHBV. The reason for the increase in G' may arise from the confinement of polymer chains within the C30B layers. Indeed, the large increase of G' observed for PHBV/PLA/C30B nanocomposite compatibilized with 5 wt% of PHBVMA melts at low frequencies with the formation of a quasi-plateau is generally interpreted as the result of both the confinement effect and the interparticle interactions [40]. The interparticle interactions come from frictional interactions between the tactoids which are predominant at low frequencies. This suggests a pseudo-solid behavior for the compatibilized nanocomposite. This is pictured as a well structured nanocomposite revealing the good dispersion of the platelets in the matrix [41].

CONCLUSION

The results reported in this article show the effect of C30B with and without PHBVMA compatibilizer on the properties of PHBV/PLA blends prepared by melt processing.

The incorporation of C30B contributes to enhance the thermal stability of PHBV, PLA and PHBV/PLA blends, as usually observed when clay is homogeneously dispersed. Besides, C30B also plays a positive effect on the flame retardancy of the PHBV/PLA/C30B composites, decreasing HRC, HRR, and THR of materials. PHBV/PLA/C30B nanocomposites exhibit improved mechanical properties in terms of Young's modulus, comparatively to PHBV/PLA blend, especially when PHBV is previously compatibilized. Last, the rheological study reveals a significant increase of the complex viscosity, the storage and the loss modulus by the addition of C30B in the PHBV/PLA blend. This is particularly noticeable when samples are submitted to low shear frequency. Moreover, this increase in the rheological response is much more pronounced in the presence of a compatibilizer as PHBVMA.

Biopolymers like PHBV or PLA often have inferior properties compared with commodity polymers. This article highlights that biopolymer blending is an efficient and promising way to improve properties and achieve some property combinations required for specific applications. The use of nanofillers and/or compatibilizers can constitute a supplementary approach to more finely tuned functional properties of biopolymer blends.

ACKNOWLEDGMENTS

The authors are pleased to express their grateful acknowledgements to Dr. Isabelle Pillin, Dr. Mickael Castro, Dr. Abdelkader Bendahou, Antoine Kervoelen, Anthony Magueresse, Françoise Peresse, and Solenn Corre for their help in the experimental work.

REFERENCES

1. S.S. Ray and M. Bousmina, *Prog. Mater. Sci.*, **50**, 962 (2005).
2. L. Zaidi, M. Kaci, S. Bruzaud, A. Bourmaud, and Y. Grohens, *Polym. Degrad. Stab.*, **95**, 1751 (2010).
3. S. Bruzaud and A. Bourmaud, *Polym. Test.*, **26**, 652 (2007).
4. Y.M. Corre, S. Bruzaud, J.L. Audic, and Y. Grohens, *Polym. Test.*, **31**, 226 (2012).
5. L.T. Lim, R. Auras, and M. Rubino, *Prog. Polym. Sci.*, **33**, 820 (2008).
6. S. Chardron, S. Bruzaud, B. Lignot, A. Elain, and O. Sire, *Polym. Test.*, **29**, 966 (2010).
7. J.W. Park, Y. Doi, and T. Iwata, *Biomacromolecules*, **5**, 1557 (2004).
8. M. Zhang and N. Thomas, *Adv. Polym. Technol.*, **30**, 67 (2011).
9. G. Thibaut and T. Budtova, *Eur. Polym. J.*, **48**, 1110 (2012).
10. I. Zembouai, M. Kaci, S. Bruzaud, A. Benhamida, Y.M. Corre, and Y. Grohens, *Polym. Test.*, **32**, 842 (2013).
11. S.S. Ray and M. Bousmina, *Macromol. Rapid Commun.*, **26**, 1639 (2005).
12. Y.S. Lipatov, *Prog. Polym. Sci.*, **27**, 1721 (2002).
13. J.H. Wu, M.S. Yen, M.C. Kuo, C.P. Wu, M.T. Leu, C.H. Li, and F.K. Tsai, *J. Appl. Polym. Sci.*, **128**, 487 (2013).
14. T. Gcwabaza, S.S. Ray, W.W. Focke, and A. Maity, *Eur. Polym. J.*, **45**, 353 (2009).
15. M. Kumar, S. Mohanty, S.K. Nayak, and M.R. Parvaiz, *Bio resour. Technol.*, **101**, 8406 (2010).
16. J.S. Hong, Y.K. Kim, K.H. Ahn, S.J. Lee, and C. Kim, *Rheol. Acta*, **46**, 469 (2007).
17. J.S. Hong, H. Namkung, K.H. Ahn, S.J. Lee, and C. Kim, *Polymer*, **47**, 3967 (2006).
18. S.S. Ray, S. Pouliot, M. Bousmina, and L.A. Utracki, *Poly mer*, **45**, 8403 (2004).

19. L. Zaidi, S. Bruzaud, A. Bourmaud, P. Mederic, M. Kaci, and Y. Grohens, *J. Appl. Polym. Sci*., **116**, 1357 (2010).
20. E. Hablot, P. Bordes, E. Pollet, and L. Avérous, *Polym. Degrad. Stab*., **93**, 413 (2008).
21. I. Zembouai, S. Bruzaud, M. Kaci, A. Benhamida, Y.M. Corre, Y. Grohens, A. Taguet and J.M. Lopez Cuesta, *J. Polym. Environ*., DOI: 10.1007/s10924 013 0626 7.
22. Y.S. Salim, A.A. Abdullah, C.S. Sipaut, M. Nasri, and M.N.M. Ibrahim, *Biores. Technol*., **102**, 3626 (2011).
23. M. Avella, G. Bogoeva Gaceva, A. Buzarovska, M.E. Errico, G. Gentile, and A. Grozdanov, *J. Appl. Polym. Sci*. **104**, 3192 (2007).
24. M.A. Abdelwahab, A. Flynn, B.S. Chiou, S. Imam, W. Orts, and F. Chiellini, *Polym. Degrad. Stab*., **97**, 1822 (2012).
25. M. Gelfer, C. Burger, A. Fadeev, I. Sics, B. Chu, and B.S. Hsiao, *Langmuir*, **20**, 3746 (2004).
26. S.S. Ray and M. Okamoto, *Prog. Polym. Sci*., **28**, 1539 (2003).
27. M. Bruzaud, Y. Grohens, S. Ilinca, and J.F. Carpentier, *Macromol. Mater. Eng*., **290**, 1106 (2005).
28. R.E. Lyon and R.N. Walters, *J. Anal. Appl. Pyrolysis*, **71**, 27 (2004).
29. H. Qin, Q. Su, S. Zhang, B. Zhao, and M. Yang, *Polymer*, **44**, 7533 (2003).
30. S. Wang, Y. Hu, R. Zong, Y. Tang, Z. Chen, and W. Fan, *Appl. Clay Sci*., **25**, 49 (2004).
31. B. Li and J. He, *Polym. Degrad. Stab*., **83**, 241 (2004).
32. R. Kozlowski and M. Wladyka Przybylak, *Polym. Adv. Technol*., **19**, 446 (2008).
33. Y. He, B. Zhu, and Y. Inoue, *Prog. Polym. Sci*., **29**, 1021 (2004).
34. J.K. Mishra, K.J. Hwang, and C.S. Ha, *Polymer*, **46**, 1995 (2005).
35. X. Liu and Q. Wu, *Polymer*, **42**, 10013 (2001).
36. K.H. Wang, M.H. Choi, C.M. Koo, Y.S. Choi, and I.J. Chung, *Polymer*, **42**, 9819 (2001).
37. B. Finnigan, D. Martin, P. Halley, R. Truss, and K. Campbell, *Polymer*, **45**, 2249 (2004).
38. H.A. Stretz, D.R. Paul, R. Li, H. Keskkula, and P.E. Cassidy, *Polymer*, **46**, 2621 (2005).
39. N. Najafi, M.C. Heuzey, and P.J. Carreau, *Comp. Sci. Tech nol*., **72**, 608 (2012).
40. N. Touati, M. Kaci, H. Ahouari, S. Bruzaud, and Y. Grohens, *Macromol. Mater. Eng*., **292**, 1271 (2007).
41. A. Durmus, A. Kasgoz, and C.W. Macosko, *Polymer*, **48**, 4492 (2007).